Journal of Catalysis 405 (2022) 534–544

Contents lists available at ScienceDirect

Journal of Catalysis

journal homepage: www.elsevier.com/locate/jcat

Influence of atmosphere, interparticle distance and support on the stability of silver on α-alumina for ethylene epoxidation

Petra H. Keijzer [1], Jeroen E. van den Reijen [1], Claudia J. Keijzer, Krijn P. de Jong, Petra E. de Jongh *

Materials Chemistry and Catalysis, Debye Institute for Nanomaterials Science, Utrecht University, Utrecht, the Netherlands

ARTICLE INFO

Article history:
Received 9 June 2021
Revised 11 November 2021
Accepted 13 November 2021
Available online 19 November 2021

Keywords:
Stability
Silver
Macroporous α-alumina
High surface area
Ethylene epoxidation
Ostwald ripening

ABSTRACT

The stability of supported metal particles is an important parameter in heterogenous catalysis. For silver catalysts supported on α-alumina, industrially used in ethylene epoxidation, the loss of silver surface area as result of particle growth is one of the most important deactivation mechanisms. In this work, the growth of silver particles was investigated by exposing catalysts to thermal treatments. The presence of oxygen during heating strongly enhanced particle growth, and the interparticle distance was a crucial parameter. However, restricting movement of complete silver particles using cage-like α-alumina did not limit particle growth. These findings indicate that Ostwald ripening was the dominant mechanism behind particle growth, with the diffusion of oxidized silver species being a rate limiting factor. Finally, higher surface area α-alumina provided better silver stability during ethylene epoxidation, with only limited decrease in selectivity. This makes silver supported on high surface area α-alumina promising candidates for ethylene epoxidation catalysis.

1. Introduction

The activity of catalysts gradually decreases over time. By gaining information on how deactivation occurs, the stability of the catalyst, and thus the life time can be improved [1,2]. Most deactivation of supported catalysts results from the loss of active surface area, which can be chemically, mechanically or thermally induced [2–5]. One example of the thermally induced loss of active surface area is the growth of the active metal particles. For α-alumina supported silver catalysts, used for the epoxidation of ethylene, this is one of the most important deactivation mechanisms [6–8].

Silver is the sole metal commercially used as catalyst for the epoxidation of ethylene [9–11]. The product, ethylene oxide, is the main building block for ethylene glycol, an intermediate for the production of antifreeze, solvents and plastics, and is produced on global scale with a yearly production of 35 million tons [11,12]. The mild oxidation properties of silver allow selective oxidation of the ethylene into ethylene oxide, instead of fully oxidizing ethylene to carbon dioxide and water [13–16]. The activity of the silver is particle size dependent, as the turnover frequency increases with the particle size up to circa 60 nm [17–20]. Above this size, the turnover frequency is constant, which makes 60 nm the optimum size for the silver particles.

The silver particles are generally supported on α-alumina with a low specific surface area (circa 1 $m^2\ g^{-1}$) [10,21–24]. The low density of hydroxyl groups present on the surface of α-alumina is beneficial in terms of selectivity, as the undesirable further conversion of ethylene oxide to CO_2 and water is relatively easy, and is facilitated by these hydroxyl groups [16,25–27]. The combination of the low density of hydroxyl groups on the surface and the low specific surface area of α-alumina minimizes the amount of these hydroxyl groups [28]. However, the low surface area of the support, especially in combination with the harsh ethylene epoxidation reaction conditions and the relatively low Tamman temperature of silver (circa 340 °C), makes the silver particles vulnerable to growth [19]. Therefore, instead of having silver particles with the optimal size of circa 60 nm, particle sizes in the range of 100–1000 nm are more common in industrial catalysts [21,22].

Particle growth results from the inherent thermodynamic instability of small metal particles distributed over the support at elevated temperatures and/or pressures [4]. In order to minimize the particle growth, it is crucial to understand the underlying mechanism. For most chemical reactions, the growth of metal particles can be ascribed to either Ostwald ripening or particle diffusion and coalescence. In Ostwald ripening, particle growth is driven by the interparticle transport of mobile metal-containing species [29,30]. The transport of these species can both take place

* Corresponding author.
E-mail address: P.E.deJongh@uu.nl (P.E. de Jongh).
[1] These authors contributed equally.

https://doi.org/10.1016/j.jcat.2021.11.016
0021-9517/

via the gas/liquid phase or via the support surface. As result of the difference in surface energy between smaller and larger particles, due to the larger specific surface area of the smaller particles, there is a net transfer of these mobile species from smaller particles to larger ones, leading to the disappearance of the smaller particles and the growth of the larger particles [29–31]. Using catalysts with a narrow particle size distribution decreases the driving force for Ostwald ripening, and hence improves the stability of the metal particles [32–36].

For particle diffusion and coalescence, the particle growth is a result of the mobility of complete metal particles. The particles diffuse over the surface of the support material and when two particles are in close proximity, they merge to form one larger particle [29]. The driving force behind coalescence is the decrease in surface energy, as the overall surface-to-volume ratio is decreased when two particles merge [35,37]. An efficient strategy against particle growth via this mechanism is decreasing the chance that two particles come close enough to merge. Therefore, one method to limit the coalescence is trapping the metal particles in the pore network of the support material [2,38]. Another method is by increasing the interparticle distance, for instance by decreasing the metal weight loading or by increasing the specific surface area of the support [32,39].

To gain insight into to which particle growth mechanism is dominant, model systems are essential. Next to having a high level of control over the particle size and size distribution, having control over the specific surface area and pore structure of the used support materials is important. Support materials with ordered, well-defined and monodisperse pore structures allow for advanced characterization methods and the possibility to deconvolute the metal induced effects from the support morphology effects [39–42]. Thanks to the use of model catalysts, the mechanism behind particle growth is now fairly well understood for many systems containing supported metal particles [34,39,43,44]. One example is the growth of copper particles supported on silica, where after carefully tuning both the ordered pores of the support material, and the particle size distribution of the copper, the dominant growth mechanism under specific conditions was identified [34]. However, the dominant mechanism behind the particle growth of supported silver particles in the epoxidation of ethylene is still under debate [45–48]. Recently, in an advanced electron microscopy study on the silver dispersion during ethylene epoxidation, particle growth via Ostwald ripening was put forward [49].

In this work, we systematically investigate which parameters influence the mobility of silver on α-alumina for the epoxidation of ethylene, by analysis of particle growth after subjecting the catalysts to thermal treatments under various conditions. Besides commercially available α-alumina support materials, we also made use of porous, ordered α-alumina materials with a high specific surface area that was recently described [50]. This material is an excellent model support for investigating the stability of supported silver particles, especially since the cage and window sizes of the pores present in the α-alumina are adjustable. Finally, next to the thermal treatments, also the catalytic performance of these materials in the epoxidation of ethylene is investigated.

2. Materials and methods

2.1. Macroporous α-alumina

Three different types of α-alumina materials were used as support. Next to the commercially available α-alumina materials from Sigma–Aldrich (1 m^2 g^{-1}, 100 mesh) and BASF (8 m^2 g^{-1}, Al-4196E), ordered macroporous α-alumina was synthesized. This α-alumina was prepared by making use of a sacrificial polymer template, according to the procedure described before [50]. The polymer template was prepared via surfactant free emulsion polymerization of methyl methacrylate (MMA, 99%, ≤30 ppm 4-methoxyphenol inhibitor, Sigma-Aldrich) in water. In a typical synthesis, 400 mL demineralized water and MMA (2.3, 1.4 and 0.9 mol L^{-1} for spheres with a number-averaged diameter of 400, 315 and 280 nm, respectively) were stirred in a 1 L round bottom flask by an overhead stirrer at 500 rpm. The emulsion was heated to 80 °C and nitrogen was bubbled through the emulsion for at least 30 min. Thereafter, potassium persulfate (initiator, KPS, 8.4 μmol L^{-1}, 99+%, Emsure) was added. The emulsion was left to react for 3 h at 80 °C after which a white dispersion had formed. The dispersion was allowed to cool down to room temperature and was filtered to remove larger chunks of polymer. The filtrate was centrifuged for 1 h at 400 rcf (relative centrifugal force) during which a white solid precipitated. The clear supernatant was decanted, and the obtained white powder was left to dry for several days at room temperature in air after which it was crushed into a powder. 1.5 g of polymeric template consisting out of stacked poly(methyl methacrylate) (PMMA) spheres is placed in a Büchner funnel. The template was alternatingly impregnated with 3 mL of a 1 M aluminum hydroxide nonahydrate (99+%, Acros) solution in demineralized water/methanol (1:1 vol ratio) and 3 mL of an ammonia (28–30 wt%, Emsure)/methanol (99.9%, VWR) mixture (1:1 vol ratio). After each impregnation step the template powder was left for 2 min to soak in the solution, then the powder was dried under vacuum for 20 min. The impregnation was performed three times with each mixture and afterward the powder was left to dry overnight at room temperature in air. The dried powder was heated under a nitrogen flow of at least 0.5 L min^{-1} (GHWV = 20 L $g^{-1}_{template}$ hr^{-1}) to 1150 °C for 6 h (heating ramp 5 °C), before the material was cooled down and heat treated again under air, using the same flow and temperature settings. The pore size of the material was adjusted by changing the sphere size in the polymer template, templates containing PMMA spheres with a diameter of 400, 315 and 280 nm were used.

2.2. Silver deposition

Silver was deposited on the α-alumina materials via incipient wetness impregnation, following a literature procedure [17,51]. The silver precursor, silver oxalate, was freshly prepared each time. Silver oxalate was synthesized by mixing an aqueous solution of oxalic acid dihydrate (99.5%, Merck) with an aqueous solution of silver nitrate (99+%, Sigma–Aldrich) (1:2 mol ratio). Next, the silver oxalate was obtained via centrifugation and washed three times with milliQ water (1:20 vol ratio) to remove any unreacted silver nitrate. Finally, the silver oxide was dried overnight in static air at 60 °C. The support powders (38–400 μm) were dried under vacuum at 120 °C for 2 h before they were impregnated with a solution (90% of the pore volume) of silver oxalate in demineralized water/ethylene diamine (99%, Sigma–Aldrich) (1:0.73 vol ratio) to obtain materials with a theoretical loading of 0.6, 4.5 or 15 wt % silver. The materials were dried overnight in air at 60 °C and after 5, 10 and 30 min of drying, the materials were thoroughly mixed. The precursor was decomposed via a heat treatment at 215 °C (2 h, 5 °C min^{-1} heating ramp) in oxygen, hydrogen or nitrogen flow (see Section 3.2, Table 2).

2.3. Characterization

The pore volume and surface area of the α-alumina materials were analyzed using N_2-physisorption. Isotherms were measured at −196 °C on a Micromeritics TriStar 3000 apparatus. The specific surface area of the support was calculated using the BET equation ($0.05 < p/p0 < 0.25$). The surface density of acid sites on the α-

alumina materials was determined by temperature programmed desorption (TPD) of ammonia, using an Autochem II 2920 V4.03 apparatus from Micromeritics. Prior to the TPD measurement, circa 100 mg α-alumina was treated at 400 °C in air for 15 min (50 mL min^{-1}), then treated to 10% ammonia in helium for 20 min at 100 °C (25 mL min^{-1} STP). For the TPD measurement, the sample was heated from 100 to 550 °C (10 °C min^{-1} heating ramp) in a helium flow (25 mL min^{-1}). The amount of desorbed ammonia was monitored using a thermal conductivity detector (TCD) and used to calculate the total amount of acid sites. For this, the complex peak shape was deconvoluted and fitted with three gaussian peaks, of which the total area was used to calculate the surface density of acid sites. The support materials and silver containing materials were analyzed by scanning electron microscopy (SEM) using a FEI XL30 FEG and Helios microscope operated at 5–10 kV. SEM samples were prepared by attaching the sample powder to the sample holder by sticky carbon tape. Prior to the measurements, a 7.5 nm platinum layer was deposited over the sample via sputter coating. Using the SEM images, the silver particles were identified and their diameter was determined manually. For this we counted for each sample at least 200 different particles in at least three different places. The surface-averaged particle sizes ($d_{p,s}$) and the standard deviations in the width of the particle size distribution ($\sigma_{p,s}$) were calculated using the following Eq. (1).

$$d_{p,s} \pm \sigma_{p,s} = \frac{\sum_{i=1}^{n} d_i^3}{\sum_{i=1}^{n} d_i^2} \pm \sqrt{\frac{1}{n} \cdot \sum_{i=1}^{n} (d_{p,s} - d_i)^2} \quad (1)$$

In this equation, n is the number of silver particles counted, and d_i the size of particle i. The interparticle distance (i_{pd}), the distance between the edges of two silver particles, was estimated using the average density of silver distributed over the surface area of the support materials and calculated using Eq. (2).

$$i_{pd(edgetoedge)} = \sqrt{\frac{A}{N}} - d_{p,s} \quad (2)$$

A is the specific surface area of the support material obtained via N_2-physisorption and N is the estimated amount of silver particles present, calculated using the silver loading and the surface-averaged silver particle size. A flat support surface and a hexagonal arrangement of spherical silver particles over the support surface were assumed. Due to the morphology of the macroporous materials, the use of electron microscopy is challenging. Therefore, to validate the SEM measurements, Diffuse-Reflectance Ultraviolet/Visible (DR UV/Vis) spectroscopy was used to determine the surface-averaged silver particle size. DR UV/Vis spectra of the materials were obtained by measuring circa 20–100 mg material in the range of 800–200 nm with a 4 nm interval and a 4 nm slit size using a Varian CARY 500 scan UV/Vis-NIR or a Perkin Elmer Lambda 950S UV/Vis-NIR spectrophotometer with an integrating sphere detector. Some of the macroporous materials were diluted, by mixing 30 mg of analyte with 600 mg pristine α-Al_2O_3 (1 m^2 g^{-1}, 100 mesh, Sigma-Aldrich). The peak position of the surface plasmon resonance absorption (λ_{max}) was used as a measure for the surface-averaged particle size using Eq. (3).

$$\lambda_{max} = 0.0073 \cdot {d_{p,s}}^2 + 0.2965 \cdot d_{p,s} + 385.34 \quad (3)$$

For this calibration curve, simulations were made using Lumerical software, for silver particles in an environment of 60% air and 40% α-alumina [17]. Macroporous α-alumina materials exhibit a relatively weak scattering peak [50], this contribution was neglected in the estimation of the silver particle size via UV/Vis. Crystal phase analysis was performed using X-Ray Diffraction (XRD) on a Bruker D2 Phaser diffractometer, equipped with a Co K_α source (λ = 0.1789 nm). The composite structures were analyzed by comparing the XRD diffractograms with crystal structures from the PDF-4 + 2016 database.

2.4. Thermal stability

Thermal stability measurements were performed in a tubular oven by heating 10 to 100 mg of silver containing material (38–150 μm) in a hydrogen or oxygen flow with a GHSV of 16,000–60,000 hr^{-1}. The samples were heated from room temperature to 100, 200, 300 and/or 400 °C with a 5 °C min^{-1} heating ramp.

2.5. Catalytic testing

The catalytic performance of the silver supported on α-alumina materials was investigated for the epoxidation of ethylene. In a typical catalysis experiment, 25 mg catalyst grains (38–150 μm) diluted with 125 mg SiC (Alfa Aesar, >98%, 212–245 μm) was loaded in a plug flow reactor with an internal diameter of 4 mm between two layers of quartz wool. The SiC diluent was washed with HNO_3 (aq) (65%, AnalaR NORMAPUR® analytical reagent; 10 mL g_{SiC}^{-1}) and calcined at 800 °C, to remove any metal or organic contaminants. The catalysts were conditioned by heating them to 270 °C for 90 min in a flow of 20 mL min^{-1} containing 7.5% ethylene and 2.13% oxygen in helium at atmospheric pressure. Afterward, the reaction temperature was lowered to 180–200 °C and the gas flow rate per gram of silver was varied between 350 and 1600 L g_{Ag}^{-1} h^{-1}. The reaction products were analyzed every 15 min using online gas chromatography (Interscience) equipped with two separate channels containing a Porabond Q column and a Molsieve 5 Å column and thermal conductivity detectors. Conversion and selectivity data were calculated from data retrieved at 180 and 200 °C when steady state was reached after 50 h on stream. For calculations on transport limitations, see Supplementary Information, Section A. See Supplementary Information, Section E for an overview of the catalytic data including the reaction time, reaction temperature, gas flow rate, conversion, selectivity and apparent TOF. The conversion of ethylene and selectivity towards ethylene oxide during the ethylene epoxidation reaction were calculated using Eqs. (4) and (5).

$$X_{Ethylene} = \frac{0.5 \cdot p_{CO_2} + p_{Ethyleneoxide} + p_{Acetaldehyde}}{p_{Ethylene,out} + 0.5 \cdot p_{CO_2} + p_{Ethyleneoxide} + p_{Acetaldehyde}} \cdot 100\% \quad (4)$$

$$S_{Ethyleneoxide} = \frac{p_{Ethyleneoxide}}{0.5 \cdot p_{CO_2} + p_{Ethyleneoxide} + p_{Acetaldehyde}} \cdot 100\% \quad (5)$$

X and S stand for the conversion (in %) and selectivity (in %) respectively, while p_A is the partial pressure of component A (in Pa). The carbon balance (Eq. (6)) was above 99% for all datapoints used.

$$Carbonbalance = \frac{p_{Ethylene,out} + 0.5 \cdot p_{CO_2} + p_{Ethyleneoxide} + p_{Acetaldehyde}}{p_{Ethylene,in}} \cdot 100\% \quad (6)$$

The apparent turnover frequency (TOF), in mole of ethylene converted per mole surface silver per second, was determined using Eq. (7).

$$TOF = \frac{P \cdot u_{Ethylene} \cdot X_{Ethylene}}{R \cdot T} \cdot \frac{1}{m_{Ag} \cdot \frac{6 \cdot V_{Agatom}}{A_{Agatom} \cdot d_{p,s}}} \quad (7)$$

P is the pressure (101325 Pa), u is the flow velocity of ethylene (in m^3 s^{-1}), X is the ethylene conversion (in %), R is the gas constant (8.314 J mol^{-1} K^{-1}), T is the ambient temperature (298 K), m is

the mass of silver used (in mol), $V_{Ag\ atom}$ the volume of a silver atom (in m^3), $A_{Ag\ atom}$ the surface area of a silver atom (in m^2) and $d_{p,s}$ is the surface-averaged diameter of the silver particles (in m), used to calculate the dispersity. Both for the volume and surface area of the silver atoms, the silver atom radius of $1.44 \cdot 10^{-10}$ m was used, the silver particles were assumed to be spherical and the silver surface atoms were assumed to be the active sites [17,28,52]. Note that the term "apparent TOF" is used as each silver surface atom is assumed to be equivalent to one active site. It is unlikely that this correlation is one-to-one, given the complex mechanism in which the available of oxygen at the surface or subsurface plays an important role, but it is a convenient measure as in general the activity is found to scale with the number of silver surface atoms. The first part of Eq. (7) was used for determining the amount of ethylene converted (in mol s^{-1}), and the bottom of the last part was used to estimate the silver surface (in mol).

3. Results and discussion

3.1. α-alumina materials

Different α-alumina materials, varying in porosity and specific surface area, were used as support material. Fig. 1 shows the N_2-physisorption isotherms (Frame A) and scanning electron microscopy (SEM) images (Frame B–F) of the selected α-alumina materials. Frame B and C are images of two commercially available α-alumina materials without intraparticle porosity, distinguished by their specific surface area of 1 $m^2\ g^{-1}$ and 8 $m^2\ g^{-1}$, respectively. Large, nonporous particles are visible in the image of 1 $m^2\ g^{-1}$ α-alumina (Frame B). Some smaller crystallites decorate the surface, but most of the material consists of large particles exceeding several micrometers. The large particles have flat surfaces and relatively sharp edges, indicative of a high crystallinity. The 8 $m^2\ g^{-1}$ α-alumina (Frame C) is a specialty chemical. The crystallites in this α-alumina consist of interconnected grains of approximately 100 to 500 nm in size, which exhibit more rounded features.

In addition to the commercially available materials, we synthesized a series of macroporous materials with much larger specific surface areas (Fig. 1, Frames D–F). X-ray diffraction (XRD) showed that all materials had the α-alumina crystal structure (see Supplementary Information, Fig. B1). According to N_2-physisorption measurements, all materials had specific surface areas of circa 30 $m^2\ g^{-1}$, which is significantly higher than the commercial α-alumina materials. These high surface areas are ascribed to the intraparticle porosity. For all macroporous materials, regular features that are arranged in a hexagonal lattice are observed. The morphology is a highly ordered pore structure, consisting of cages with interconnecting windows to the nearby cages. Using SEM, the cage and window sizes were measured. The cage and the window sizes vary per material, the cage size ranges from 160 nm to 205 and the window size ranges from 55 to 115 nm.

Hydroxyl groups on the surface of the alumina (acid sites) facilitate the unwanted combustion of ethylene oxide to CO_2 and water and therefore influence the selectivity of the catalysts [16,25–27]. The acidity of the α-alumina materials was determined using temperature programmed desorption (TPD) of ammonia. The desorption curves and the data fitting used to calculate the surface density of acid sites are given in Supplementary Information, Fig. B2, and an overview of the specific surface areas and the surface density of acid sites of the materials are given in Table 1. The amount of acid sites per surface area was very similar for all alumina supports discussed and in line with values reported in literature [53,54], except for the 1 $m^2\ g^{-1}$ α-alumina. However, it should be noted that in this case the error in the determination of the acid density might be much larger than for the other alumina materials, as the main error is in the determination of the specific surface area.

3.2. Silver deposition

The size of the silver particles deposited on the α-alumina materials was tuned by varying the gas atmosphere in the heat treatment step [17]. In this way, despite the use of different support materials and metal weight loadings, sets of supported silver particles with the same initial silver particle sizes were prepared, and all materials were exposed to the same maximum temperature during preparation. XRD showed that irrespective of the atmosphere used during the heat treatments, all materials showed the diffraction lines of metallic silver (see Supplementary Information, Fig. B3). This can be explained by the low decomposition temperatures of circa 200 °C for silver (I) oxide and below 200 °C for silver (I,III) oxide [55]. It is known that under these conditions some small particles of silver oxide or surface oxides may still be formed and be stable up to higher temperatures, however, the bulk of the particles is metallic [20,56–58].

Silver particle size analysis was performed both by using SEM and Diffuse-Reflectance (DR) UV/Vis. In the SEM images in Fig. 2, the silver is visible as bright white, round particles, deposited on 30 $m^2\ g^{-1}$ α-alumina with cage and window size of respectively 205 and 115 nm (Frame A) and on non-porous 1 $m^2\ g^{-1}$ α-alumina (Frame B). The insets of these images show the particle size distributions, UV/Vis spectra of these materials are given in Frame C. As the supported silver particles are large enough to exhibit surface plasmon resonance, the position and intensity of the Ag surface plasmon resonance peaks in UV/Vis spectroscopy can be used to derive a surface-averaged silver particle size [17,59–61]. The surface-averaged silver particle sizes obtained from the maximum peak positions, 45 nm for the silver on 30 $m^2\ g^{-1}$ α-alumina and 52 nm for the silver on 1 $m^2\ g^{-1}$ α-alumina, are in agreement with the surface-averaged silver sizes obtained from the SEM measurements, 45 nm ± 22 nm, and 44 nm ± 22 nm, respectively. An overview of all materials discussed in this paper is given in Table 2.

3.3. Silver thermal stability

Catalyst deactivation is typically slow, significant deactivation may take months to years [8,62,63]. Investigating the deactivation process under industrially relevant conditions is therefore time consuming. To accelerate the deactivation, materials can be exposed to harsh conditions. In this study, the particle growth was accelerated by heating the silver containing materials to relatively high temperatures. The stability of the silver is then investigated by measuring the particle size of the supported silver particles before and after subjecting the materials to these heat treatments.

3.3.1. Reductive versus oxidative atmosphere

First of all, the influence of the gas atmosphere during the heat treatment on the growth of the silver particles was investigated. The supported silver particles were subjected to heat treatments in oxidative or reductive atmosphere, as these represent conditions present during oxidation or reduction reactions. Heat treatments in inert atmosphere were not performed, as during catalyst preparation, the size of the silver particles obtained in inert atmosphere was in-between those of reductive and oxidative atmosphere. Fig. 3 shows the silver particle size distributions of $15Ag40/8Al_2O_3$ before and after an additional heat treatment at 200 °C or 400 °C, under reductive atmosphere (Frame A) or oxidative atmosphere (Frame B). Frame C gives an overview of the surface-averaged silver particle sizes after each heat treatment.

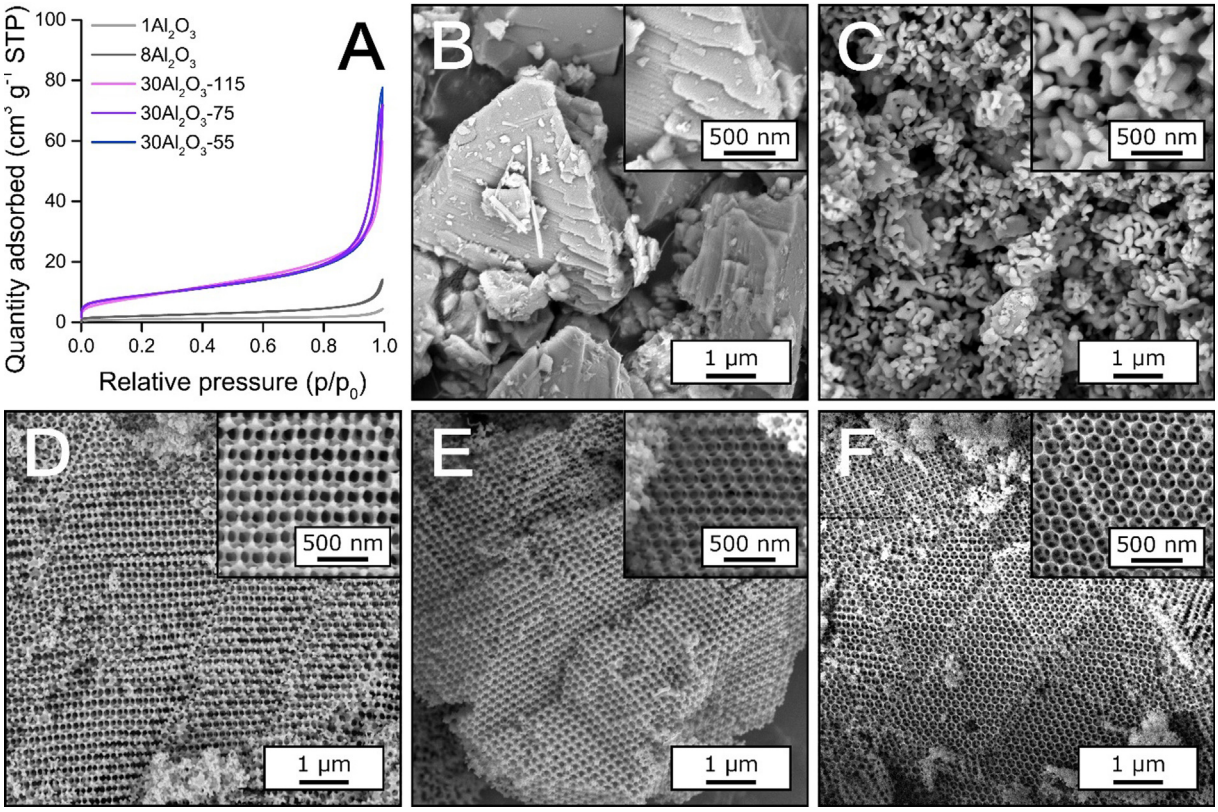

Fig. 1. Isotherms measured using N_2-physisorption (A) and the corresponding scanning electron microscopy images (B-F) of the various α-alumina materials. B: 1 m^2 g^{-1} α-alumina; C: 8 m^2 g^{-1} α-alumina; D - F: ordered macroporous α-alumina with specific surface areas of circa 30 m^2 g^{-1} and number-averaged cage and window sizes of respectively 205 and 115 nm (D), 165 and 75 nm (E) and 160 and 55 nm (F).

Table 1
Overview of the surface density of acid sites on α-alumina materials, labeled in the form $SSAAl_2O_3$-WS, with SSA the specific surface area of the α-alumina used as support material, and WS the number-averaged window size of the α-alumina, if applicable.

Material	Specific surface area (m^2 g^{-1})	Acid sites (μmol g^{-1})	Acid sites[a] (nm^{-2})
$1Al_2O_3$	1	25.6	15
$8Al_2O_3$	8	55.7	4.2
$30Al_2O_3$-115	33	194	3.6
$30Al_2O_3$-55	31	165	3.2

[a] Density of acid sites calculated using the specific surface area of the materials.

Upon heating the supported silver particles in hydrogen, almost no growth was observed for temperatures up to 400 °C (Frames A and C, red line). Contrarily, when heated in oxygen atmosphere (Frames B and C, blue line), the size of the particles increased significantly. This shows that oxidized metal species are necessary for mobility of the metal, as was reported in literature before [8,29,32,64–66]. In a study on the stability of gold nanoparticles, it was found that an oxidizing gas atmosphere was required to create mobile species [66]. Also for silver, the formation of mobile AgO_x clusters occurred in the presence of oxygen, and cationic species were stabilized by surface and/or gas-phase species under oxidizing conditions [67,68]. This is a strong indication that particle growth takes place via the Ostwald ripening mechanism, and that

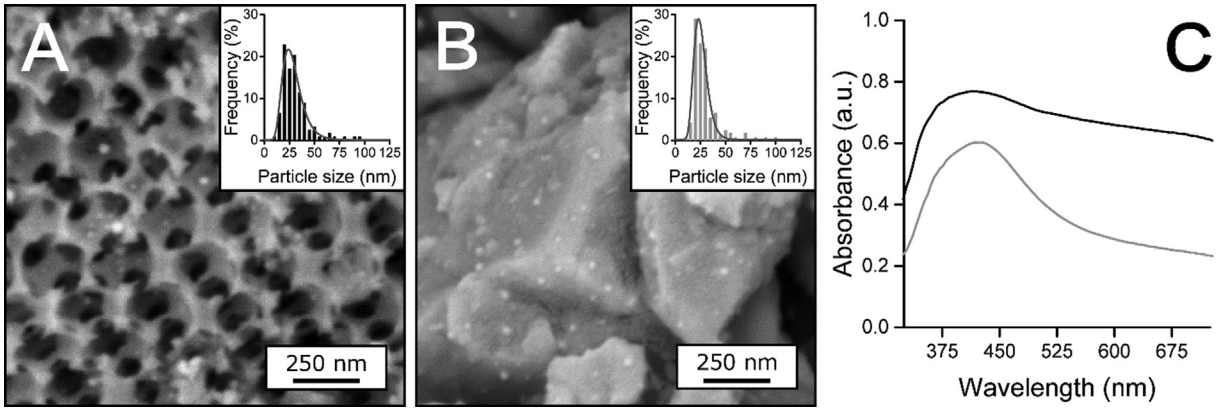

Fig. 2. SEM images of 15 wt% silver particles supported on ordered macroporous α-alumina ($15Ag45/30Al_2O_3$-115, Frame A) and non-porous α-alumina with a surface area of 1 m^2 g^{-1} ($0.6Ag45/1Al_2O_3$, Frame B) and the corresponding UV/Vis spectra in black and gray, respectively (Frame C).

Table 2
Overview of silver on α-alumina materials, labeled in the form wt%AgDd/SSAAl_2O_3-WS, with wt% being the theoretical silver weight loading, D the initial surface-averaged silver particle diameter, SSA the specific surface area of the α-alumina used as support material, and WS the number-averaged window size of the α-alumina, if applicable. For all prepared materials, the decomposition of the silver precursor during preparation was performed at 215 °C, at the gas composition listed in the second column.

Material	Gas composition during preparation	Silver		α-alumina support		
		Weight loading (wt%)	Particle size[a] (Ø, nm)	Surface area (m^2 g^{-1})	Cage size (nm)	Window size (nm)
0.6Ag45/1Al_2O_3	N_2	0.6	44 ± 22	1	-	-
15Ag60/1Al_2O_3	50% H_2 in N_2	15	63 ± 14	1	-	-
15Ag75/1Al_2O_3	50% H_2 in N_2	15	74 ± 42	1	-	-
4.5Ag45/8Al_2O_3	N_2	4.5	35 ± 17	8	-	-
15Ag40/8Al_2O_3	N_2	15	41 ± 8	8	-	-
15Ag60/8Al_2O_3	O_2	15	56 ± 29	8	-	-
15Ag75/8Al_2O_3	O_2	15	75 ± 31	8	-	-
15Ag45/30Al_2O_3-115	N_2	15	45 ± 22	33	205	115
15Ag60/30Al_2O_3-115	O_2	15	61 ± 26	33	205	115
15Ag60/30Al_2O_3-80	O_2	15	65 ± 23	30	190	80
15Ag60/30Al_2O_3-75	O_2	15	59 ± 27	32	165	75
15Ag70/30Al_2O_3-55	O_2	15	70 ± 40	31	160	55

[a]Surface-averaged particle sizes and the width of the size distributions, obtained via SEM analysis. Small variations in the experimental preparation parameters, such as batch size, batch of reactants and the use of different ovens led to some variation in the silver particle sizes.

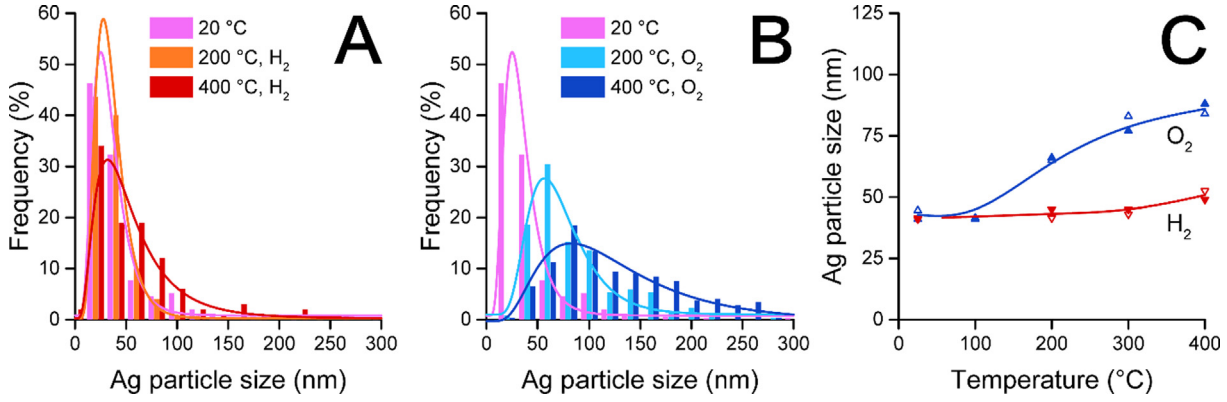

Fig. 3. Silver particle size distributions of 15Ag40/8Al_2O_3 before and after additional heat treatments at elevated temperatures in hydrogen (A) or oxygen (B) and the surface-averaged silver particle size as function of temperature (C). The surface-averaged particle sizes were determined using SEM (closed symbols) and DR UV/Vis (open symbols).

the mobile species consist of complexed silver cations [4]. The nature of these cationic species is unknown. Density functional theory (DFT) calculations showed that on copper particles for the methanol synthesis and water gas shift reaction, CuCO and Cu_2HCOO are the main transport species, but literature on the nature of silver cations is scarce [69]. Since no significant particle growth was observed in the absence of oxygen, and as for the epoxidation of ethylene the presence of oxygen is relevant, further heat treatments for exploring the thermal stability of the silver particles were performed under oxygen atmosphere.

3.3.2. Interparticle distance of silver particles

Next, the influence of support properties on the thermal stability of the silver was investigated. An important parameter is the surface area of the support, which affects also the distance between the supported silver particles for a given silver weight loading and particle size. Supported silver particles with the same initial silver particle size and weight loading were prepared on α-alumina with specific surface areas of 1, 8 or 30 m^2 g^{-1}. As a result, the estimated average interparticle distance (edge to edge) varied from 20 to 170 to 390 nm for the 1, 8 and 30 m^2 g^{-1} α-alumina materials, respectively. In Fig. 4, Frame A, the surface-averaged silver particle sizes of these catalysts are given as function of the temperature of the thermal treatment. Up to 200 °C, the surface-averaged silver particle size was similar to the initial silver particle size of 60 nm. This was expected, as they have already been heated to 215 °C during material preparation. Large differences in particle growth are observed at higher temperatures. When the silver particles were supported on α-alumina with a specific surface area of 1 m^2 g^{-1}, the particle size increased from 60 to larger than 200 nm, while particle growth was modest for the silver particles supported on the 8 m^2 g^{-1} and almost absent up to 400 °C for the particles on 30 m^2 g^{-1} α-alumina material.

It is known that interparticle distances can have a large influence on particle stability [41,70]. Based on the previous results, it is not clear whether the differences in silver particle stability were due to support properties such as specific surface area, morphology and/or the chemical nature of the surface, or due to the interparticle distance. Hence, the thermal stability of silver on these three support materials was again evaluated, but now with a constant initial average interparticle distance. For the catalysts shown in Fig. 4, Frame B, the silver weight loading was adjusted according to the specific surface area of the α-alumina. As the materials had the same initial surface-averaged particle size (45 nm) and silver surface density (30 at_{Ag} nm^{-2}), they also had a similar average interparticle distance of 120 nm. In this case, the thermal stability

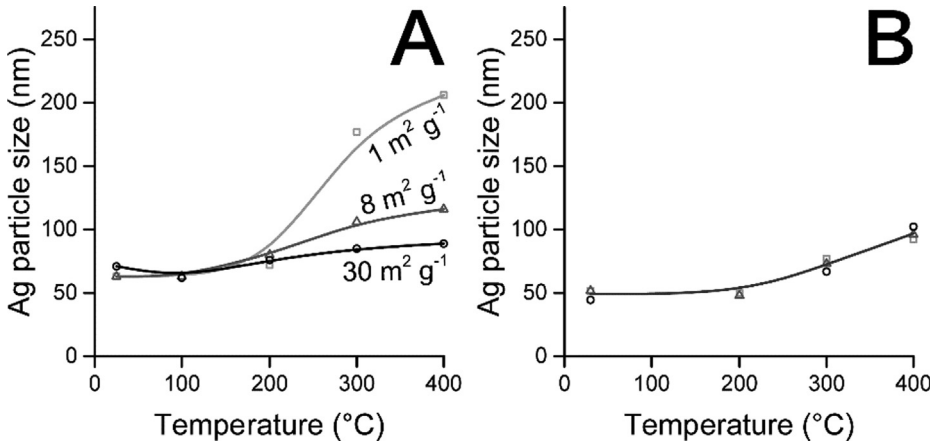

Fig. 4. Surface-averaged particle sizes (obtained using DR UV/Vis spectroscopy) of silver supported on α-alumina with specific surface areas of 1 $m^2\ g^{-1}$, 8 $m^2\ g^{-1}$ or 30 $m^2\ g^{-1}$, after heat treatment in oxygen atmosphere. In Frame A, the silver weight loading was constant (15 wt%) while the estimated average initial interparticle distance varied from 20 nm (15Ag60/1Al_2O_3, ■), via 170 nm (15Ag60/8Al_2O_3, ▲) to 390 nm (15Ag60/30Al_2O_3-80, ●). In Frame B, the weight loading of the silver was adjusted from 0.6 wt% (0.6Ag45/1Al_2O_3, ■), via 4.5 wt% (4.5Ag45/8Al_2O_3, ▲) to 15 wt% (15Ag45/30Al_2O_3-115, ●), to obtain the same estimated average initial interparticle distance of 120 nm for all three catalysts.

of the silver on the catalysts with the same interparticle distance was very similar. This shows that the interparticle distance is a crucial parameter for the stability of supported silver particles.

Interparticle distance always plays an important role in the growth via particle diffusion and coalescence. However, for the Ostwald ripening mechanism, interparticle distance only has an important influence when the diffusion of the mobile metal-containing species is a rate limiting step for particle growth, while it becomes irrelevant if the formation of these mobile species, or their annihilation by attachment to another metal particle, is rate limiting [70,71]. If growth occurs mainly via particle diffusion and coalescence, it can be slowed down by restricting the movement of complete particles [2,41]. In Fig. 4, Frame B, the size of the silver particles (45 nm) was relatively small compared to the size of the windows (105 nm) interconnecting the cages in the 30 $m^2\ g^{-1}$ α-alumina support. It is expected that these small particles could freely move through the cages of the support material. Hence, α-alumina with a smaller window size and silver particles with a larger initial size were used to restrict the movement of complete particles, and thus to investigate which particle growth mechanism was dominant.

3.4. Support pore structure and window size

In Fig. 5, silver particle sizes on three different macroporous α-alumina support materials with varying cage and window size (see Fig. 1, Frames D–F) are shown. The specific surface area of these macroporous α-alumina materials was the same (30 $m^2\ g^{-1}$), as were the silver weight loading (15 wt%) and initial silver particle size (60 nm). Therefore, also the interparticle distance for these three materials was similar. The only difference was the size of the cages and windows of the α-alumina support, with the window size ranging from 115 nm to 55 nm. Frames A and B show the particle size distributions after preparation (Frame A) and after an additional heat treatment at 400 °C (Frame B). Frame C shows the surface-averaged silver particle sizes versus the window size of the support, before and after the additional heat treatment.

For the silver particles supported on the macroporous α-alumina with window sizes of 75 or 115 nm, the surface-averaged sizes of the initial silver particles are smaller than the window sizes of the support, whereas for the α-alumina with window size of 55 nm, the initial surface-averaged particle size is larger than the window size. The surface-averaged silver particle size had increased to circa 115 nm for all three materials after the heat treatment at 400 °C. Therefore, the growth of the silver particles was not restricted by window sizes smaller than the surface-averaged particle size, as would have been expected if particle diffusion and coalescence was the major mechanism behind particle growth. Although Ostwald ripening can be described and modelled quite accurately, this is unfortunately not the case for particle diffusion and coalescence, as essential parameters for modelling particle diffusion are unknown [72]. The unrestricted particle growth while having different window sizes, combined with the results from the heat treatments where the atmosphere was varied, strongly indicate that Ostwald ripening is the major mechanism behind the particle growth of silver particles, with diffusion of metal-containing species being the rate determining step for growth.

3.5. Ethylene epoxidation

The supported silver catalysts (15 wt% Ag/α-alumina) were used in the epoxidation of ethylene. The activities of these catalysts, with apparent turnover frequencies (TOFs) in the range of 0.03–0.25 $mol_{ethylene}\ mol_{Ag,surf}^{-1}\ s^{-1}$ at 180–200 °C, were in line with activities of similar ethylene epoxidation catalysts described in literature [28,52,56,73–75]. In Fig. 6 the selectivity towards ethylene oxide versus the conversion of ethylene for silver particles supported on α-alumina with varying surface area is given. The surface-averaged size of the silver particles ranged from 60 to 75 nm. Particle size effects were not expected in this size range [17]. The interparticle distances between the silver nanoparticles had no influence on the activity of the catalysts (see Supplementary Information, Fig. C1). All catalysts showed a decrease in selectivity for higher conversion levels, as is also described and explained in previous studies [25,76–78]. The overall selectivity is highest for silver supported on the lowest surface area α-alumina (1 $m^2\ g^{-1}$), with a selectivity between 30 and 60%, up to a conversion of 4%. These obtained selectivities are in accordance with literature on unpromoted silver catalysts, where selectivities between 30 and 40% are reported [19,24,79–81]. Upon increasing the surface area of the α-alumina to 8 or 30 $m^2\ g^{-1}$, the selectivities of the catalysts slightly decreased, as result of the larger gravimetric density of acid sites present on the support materials with higher specific surface areas (see Table 1). This is in agreement with theory, as the complete combustion of the product, ethylene

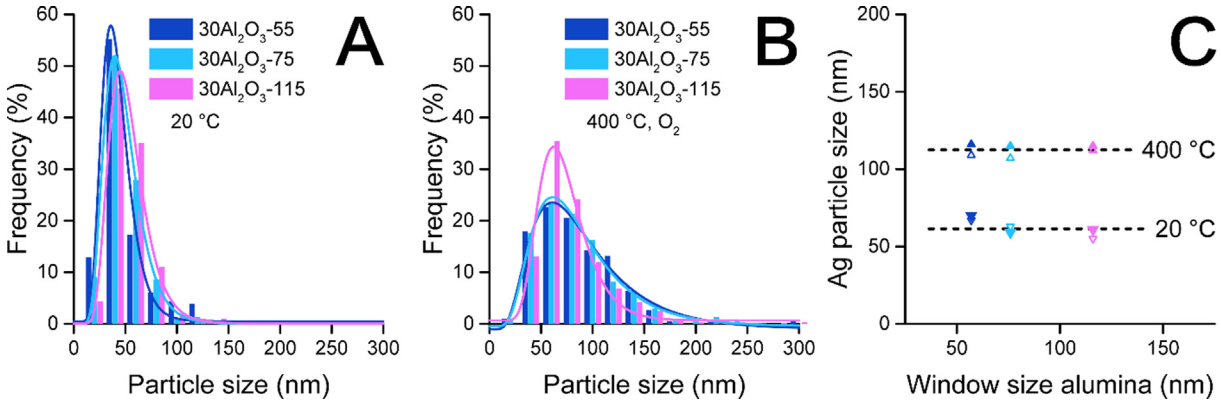

Fig. 5. Silver particle size distributions of 15Ag70/30Al_2O_3-55 (dark blue), 15Ag60/30Al_2O_3-75 (light blue), 15Ag60/30Al_2O_3-115 (pink) before (A) and after the additional heat treatments at 400 °C in oxygen atmosphere (B) and the surface-averaged particle sizes before (▼) and after heat treatment (▲) as function of the window size of the support (C). The surface-averaged particle sizes were determined using SEM (closed symbols) and DR UV/Vis spectroscopy (open symbols). (For interpretation of the references to colour in this figure legend, the reader is referred to the web version of this article.)

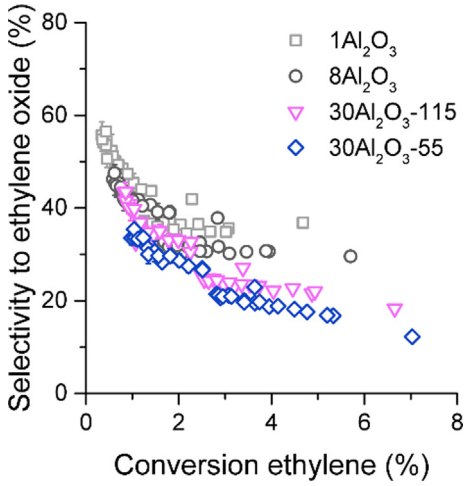

Fig. 6. Selectivity to ethylene oxide versus the ethylene conversion for a selection of catalysts (25 mg catalyst used, 15 wt% Ag): 15Ag75/1Al_2O_3 (□), 15Ag75/8Al_2O_3 (○) 15Ag70/30Al_2O_3-55 (◇), 15Ag60/30Al_2O_3-115 (▽). Different conversions were obtained over a range of 350–1600 L g_{Ag}^{-1} h^{-1} (7.5% ethylene and 2.13% oxygen in helium) at 180 or 200 °C. See Supplementary Information, Fig. C2 for more details.

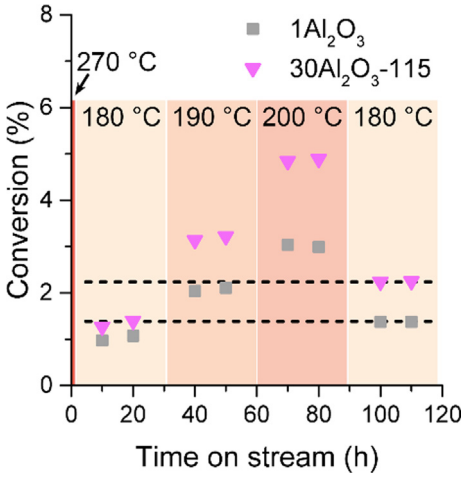

Fig. 7. Conversion of ethylene in the epoxidation of ethylene versus the time on stream for a selection of catalysts (25 mg catalyst used, 15 wt% Ag) using a gas flow rate of 350 L g_{Ag}^{-1} h^{-1} (7.5% ethylene and 2.13% oxygen in helium): 15Ag75/1Al_2O_3 (■) and 15Ag70/30Al_2O_3-115 (▼). At every temperature (180, 190 and 200 °C), the same gas flow rate was used twice, with an interval of 10 h.

oxide, is facilitated by hydroxyl groups on the surface of the support material, which decreases the overall selectivity [16,25–28].

Particle growth during accelerated aging is not the same as particle growth during the actual reaction as a result of, among others, different concentrations of oxidizing and reducing and potentially complexing species, and effective charges at the metal catalyst surface [42,82–84]. In our case, one large difference between the heat treatments and the catalytic reactions was the atmosphere. An oxidizing atmosphere was used during the heat treatments, whereas the atmosphere during catalysis contained both oxygen and reducing species, such as ethylene. Even though the stability of the silver particles under these conditions was not evaluated in depth, some conclusions can be drawn from the differences in the surface-averaged silver particle size of the catalysts before and after 120 h on stream, shown in Table 3. For the particle size distributions of these catalysts before and after catalysis, see Supplementary Information, Fig. D1.

When considering the differences between particle sizes before and after catalysis, there is only one catalyst that really stands out, which is the catalyst containing silver particles supported on 1 m^2 g^{-1} α-alumina, for which the surface-averaged silver particle size

Table 3
Overview of the surface-averaged particle size obtained using SEM of supported silver of catalysts used in the epoxidation of ethylene after 120 h on stream at 180–200 °C (90 min at 270 °C) in a flow of 350 and 1600 L g_{Ag}^{-1} h^{-1} containing 7.5% ethylene and 2.13% oxygen in helium at atmospheric pressure.

Material	Silver particle size before catalysis (Ø, nm)	Silver particle size after catalysis (Ø, nm)
15Ag75/1Al_2O_3	74	160
15Ag75/8Al_2O_3	75	80
15Ag60/30Al_2O_3-115	61	62
15Ag70/30Al_2O_3-55	70	72

of the used catalyst was twice as large as the initial surface-averaged size. For the catalyst on 8 m^2 g^{-1} α-alumina there is a slight indication of some silver particle growth, while the silver catalysts supported on higher surface area alumina seemed fully stable. Looking in detail at the silver catalyst supported on 1 m^2 g^{-1} α-alumina, the particle growth occurs during the 90 min conditioning step at 270 °C, as after that step no further deactivation is observed upon comparing the activity of the catalyst after the conditioning step and after 100 h on stream (see Fig. 7). To further

investigate the kinetics of particle growth on 1 m^2 g^{-1} α-alumina during catalysis, and its influence on the activity, isothermal runs at 230 °C or 250 °C without a conditioning step were performed (see Supplementary Information, Fig. D2). Also at these temperatures, the particle growth was severe (from 74 nm to circa 160 nm in both cases, see Supplementary Information, Fig. D3) and fast, taking place within the first 10 h of the run and hence overlapping with the activation period of the catalyst. This is in line with the fast observed growth during the heat treatments, when silver particles supported on 1 m^2 g^{-1} α-alumina with an initial size of 63 nm heated to 300 °C grew to about the same size (177 nm, 15Ag60/1Al_2O_3, Fig. 4, Frame A, heating from 200 °C to 300 °C took 20 min).

For the other catalysts, (almost) no growth of the silver particles was observed. First of all, the limited particle growth for observed in 15Ag75/8Al_2O_3 and the lack of growth in 15Ag60/30Al_2O_3-115 and 15Ag70/30Al_2O_3-55 confirms that the deactivation is indeed a slow process. Additionally, the particle growth that was observed after catalysis upholds the trends in particle growth observed upon the accelerated aging tests using heat treatments. The catalyst stability is enhanced significantly by making use of high surface area support material at limited decrease in selectivity. This shows the promise of using α-alumina with a high specific surface area as support material in the epoxidation of ethylene.

4. Conclusions

The thermal stability of silver particles supported on α-alumina depends on the gas atmosphere. In hydrogen, almost no increase in the surface-averaged silver particle size was observed at temperatures up to 400 °C, with particle growth being pronounced in the presence of oxygen. The interparticle distance was an important parameter for growth, with a higher silver stability on α-alumina materials with higher specific surface areas, for a given silver weight loading and initial particle size. Restricting movement of whole silver particles, by adjusting the support morphology, did not slow down particle growth. Based on these observations, Ostwald ripening is presumed to be the dominant particle growth mechanism, in which cationic silver complexes are the mobile species. Given that the interparticle distance is a key factor, the diffusion of these cation silver species is considered a rate determining step for particle growth. The silver particles supported on the different α-alumina materials were investigated for the epoxidation of ethylene. On the one hand, a higher surface area of the macroporous α-alumina materials led to a limited decrease in selectivity towards ethylene oxide. On the other hand, using a high surface area support provided larger interparticle distances, and hence is an excellent strategy to prevent particle growth. Support materials with high specific surface area are therefore interesting candidates for more stable catalysts in the epoxidation of ethylene.

Declaration of Competing Interest

The authors declare that they have no known competing financial interests or personal relationships that could have appeared to influence the work reported in this paper.

Acknowledgements

This research was funded by the Netherlands Center for Multiscale Catalytic Energy Conversion (MCEC), an NWO Gravitation programme funded by the Ministry of Education, Culture and Science of the government of the Netherlands and by an NWO-Vici grant (16.130.344). The authors would like to thank Eric Helleband (SEM), Hans Meeldijk (SEM), Remco Dalebout (N_2-physisorption), Yuang Piao (NH_3-TPD), Johan de Boed (UV/Vis, catalytic setup) and Jan Willem de Rijk (catalytic setup) for technical support.

Appendix A. Supplementary material

Supplementary data to this article can be found online at https://doi.org/10.1016/j.jcat.2021.11.016.

References

[1] C.T. Campbell, The energetics of supported metal nanoparticles: Relationships to sintering rates and catalytic activity, Acc. Chem. Res. 46 (8) (2013) 1712–1719, https://doi.org/10.1021/ar3003514.
[2] E.D. Goodman, J.A. Schwalbe, M. Cargnello, Mechanistic understanding and the rational design of sinter- resistant heterogeneous catalysts, ACS Catal. 7 (10) (2017) 7156–7173, https://doi.org/10.1021/acscatal.7b01975.
[3] C.H. Bartholomew, R.J. Farrauto, Fundamentals of Industrial Catalytic Processes, second ed., John Wiley & Sons, Inc, 2005. https://doi.org/10.1002/9780471730071.
[4] C.H. Bartholomew, Mechanisms of catalyst deactivation, Appl. Catal. A Gen. 212 (1-2) (2001) 17–60, https://doi.org/10.1016/S0926-860X(00)00843-7.
[5] M.D. Argyle, C.H. Bartholomew, Heterogeneous catalyst deactivation and regeneration: a review, Catalysts. 5 (2015) 145–269, https://doi.org/10.3390/catal5010145.
[6] X.E. Verykios, F.P. Stein, R.W. Coughlin, Oxidation of ethylene over silver: adsorption, kinetics, catalyst, Catal. Rev. 22 (2) (1980) 197–234, https://doi.org/10.1080/03602458008066534.
[7] A.J.F. Van Hoof, I.A.W. Filot, H. Friedrich, E.J.M. Hensen, Reversible restructuring of silver particles during ethylene Epoxidation, ACS Catal. 8 (2018) 11794–11800, https://doi.org/10.1021/acscatal.8b03331.
[8] G. Boskovic, D. Wolf, A. Brückner, M. Baerns, Deactivation of a commercial catalyst in the epoxidation of ethylene to ethylene oxide - Basis for accelerated testing, J. Catal. 224 (1) (2004) 187–196, https://doi.org/10.1016/j.jcat.2004.02.030.
[9] T.E. Lefort, Process for the Production of Ethylene Oxide, US1998878A, 1931.
[10] M. Mitsuhata, F. Watanabe, T. Kumazawa, F. Watanab, T. Kumazawa, Silver Catalyst for Production of Ehtylene Oxide, 4,368,144, 1983.
[11] L.G. Pinaeva, A.S. Noskov, Prospects for the development of ethylene oxide production catalysts and processes (Review), Pet. Chem. 60 (11) (2020) 1191–1206, https://doi.org/10.1134/S096554412011016X.
[12] TechNavio, Global Ethylene Oxide and Ethylene Glycol Market 2016–2020, TechNavio: London, United Kingdom, 2016.
[13] C.T. Campbell, M.T. Paffett, Model studies of ethylene epoxidation catalyzed by the Ag(110) surface, Surf. Sci. 139 (2-3) (1984) 396–416, https://doi.org/10.1016/0039-6028(84)90059-1.
[14] M. Mavrikakis, D.J. Doren, M.A. Barteau, Density functional theory calculations for simple oxametallacycles: trends across the periodic table, J. Phys. Chem. B 102 (1998) 394–399.
[15] M.O. Ozbek, I. Onal, R.A. van Santen, Why silver is the unique catalyst for ethylene epoxidation, J. Catal. 284 (2) (2011) 230–235, https://doi.org/10.1016/j.jcat.2011.08.004.
[16] M.O. Özbek, R.A. van Santen, The mechanism of ethylene epoxidation catalysis, Catal. Lett. 143 (2) (2013) 131–141, https://doi.org/10.1007/s10562-012-0957-3.
[17] J.E. van den Reijen, S. Kanungo, T.A.J. Welling, M. Versluijs-Helder, T.A. Nijhuis, K.P. de Jong, P.E. de Jongh, Preparation and particle size effects of Ag/α-Al_2O_3 catalysts for ethylene epoxidation, J. Catal. 356 (2017) 65–74, https://doi.org/10.1016/j.jcat.2017.10.001.
[18] J.K. Lee, X.E. Verykios, R. Pitchai, Support and crystallite size effects in ethylene oxidation catalysis, Appl. Catal. 50 (1) (1989) 171–188, https://doi.org/10.1016/S0166-9834(00)80834-9.
[19] S.N. Goncharova, E.A. Paukshtis, B.S. Bal'zhinimaev, Size effects in ethylene oxidation on silver catalysts. Influence of support and Cs promoter, Appl. Catal. A Gen. 126 (1995) 67–84.
[20] V.I. Bukhtiyarov, I.P. Prosvirin, R.I. Kvon, S.N. Goncharova, B.S. Bal'zhinimaev, XPS study of the size effect in ethene epoxidation on supported silver catalysts, J. Chem. Soc., Faraday Trans. 93 (1997) 2323–2329, https://doi.org/10.1039/a608414a.
[21] A.M. Lauritzen, Ethylene oxide catalyst and process for preparing the catalyst, US4761394, 1988. https://linkinghub.elsevier.com/retrieve/pii/0375650585900112.
[22] R.P. Nielsen, J.H. La Rochelle, Catalyst for production of ethylene oxide, US3962136, 1976.
[23] S. Rebsdat, D. Mayer, Arsenic and arsenic compounds, IARC Monogr. Eval. Carcinog. Risk Chem. Hum. 23 (1980) 39–141, https://doi.org/10.1002/14356007.a10_117.
[24] A. Ayame, Y. Uchida, H. Ono, T. Sato, H. Hayasaka, Epoxidation of ethene over silver catalysts supported on crystalline α-alumina carriers, Stud. Surf. Sci. Catal. 145 (2003) 509–510, https://doi.org/10.1016/s0167-2991(03)80283-5.
[25] O.O. Bernardini, E.A. Cherniak, Heterogeneous isomerization of ethylene oxide to acetaldehyde, Can. J. Chem. 51 (9) (1973) 1371–1377, https://doi.org/10.1139/v73-205.

[26] Y. Hui-Xing, C. Hua, H. De-Gang, The rate constant determination for the isomerization of ethylene oxide to acetaldehyde by chemical shock tube, Acta Chim. Sin. (1989) 941–946.
[27] J.K. Lee, X.E. Verykios, R. Pitchai, Support participation in chemistry of ethylene oxidation on silver catalysts, Appl. Catal. 44 (1988) 223–237, https://doi.org/10.1016/S0166-9834(00)80055-X.
[28] C.-F. Mao, M. Albert Vannice, High surface area α-aluminas III. Oxidation of ethylene, ethylene oxide, and acetaldehyde over silver dispersed on high surface area α-alumina, Appl. Catal. A, Gen. 122 (1) (1995) 61–76, https://doi.org/10.1016/0926-860X(94)00214-2.
[29] A.K. Datye, Q. Xu, K.C. Kharas, J.M. McCarty, Particle size distributions in heterogeneous catalysts: what do they tell us about the sintering mechanism?, Catal Today 111 (1-2) (2006) 59–67, https://doi.org/10.1016/j.cattod.2005.10.013.
[30] T.W. Hansen, A.T. DeLaRiva, S.R. Challa, A.K. Datye, Sintering of catalytic nanoparticles: particle migration or ostwald ripening?, Acc Chem. Res. 46 (8) (2013) 1720–1730, https://doi.org/10.1021/ar3002427.
[31] P. Munnik, M. Wolters, A. Gabrielsson, S.D. Pollington, G. Headdock, J.H. Bitter, P.E. de Jongh, K.P. de Jong, Copper nitrate redispersion to arrive at highly active silica-supported copper catalysts, J. Phys. Chem. C 115 (30) (2011) 14698–14706, https://doi.org/10.1021/jp111778g.
[32] P.J.F. Harris, Growth and structure of supported metal catalyst particles, Int. Mater. Rev. 40 (3) (1995) 97–115, https://doi.org/10.1179/imr.1995.40.3.97.
[33] I.M. Lifshitz, V.V. Slyozov, The kinetics of precipitation from supersaturated solid solutions, J. Phys. Chem. Solids 19 (1-2) (1961) 35–50, https://doi.org/10.1016/0022-3697(61)90054-3.
[34] C.E. Pompe, D.L. van Uunen, L.I. van der Wal, J.E.S. van der Hoeven, K.P. de Jong, P.E. de Jongh, Stability of mesocellular foam supported copper catalysts for methanol synthesis, Catal. Today. (2019) 1–11, https://doi.org/10.1016/j.cattod.2019.01.053.
[35] P. Wynblatt, N.A. Gjostein, Particle growth in model supported metal catalysts-I. Theory, Acta Metall. 24 (12) (1976) 1165–1174, https://doi.org/10.1016/0001-6160(76)90034-1.
[36] S. Hu, W.-X. Li, Influence of particle size distribution on lifetime and thermal stability of Ostwald ripening of supported particles, ChemCatChem 10 (13) (2018) 2900–2907, https://doi.org/10.1002/cctc.201800331.
[37] X.G. Zhou, W.K. Yuan, Modeling silver catalyst sintering and epoxidation selectivity evolution in ethylene oxidation, Chem. Eng. Sci. 59 (8-9) (2004) 1723–1731, https://doi.org/10.1016/j.ces.2004.01.028.
[38] S.H. Joo, J.Y. Park, C.-K. Tsung, Y. Yamada, P. Yang, G.A. Somorjai, Thermally stable Pt/mesoporous silica core-shell nanocatalysts for high-temperature reactions, Nat. Mater. 8 (2) (2009) 126–131, https://doi.org/10.1038/nmat2329.
[39] G. Prieto, J. Zečević, H. Friedrich, K.P. de Jong, P.E. de Jongh, Towards stable catalysts by controlling collective properties of supported metal nanoparticles, Nat. Mater. 12 (1) (2013) 34–39, https://doi.org/10.1038/nmat3471.
[40] D. Han, X. Li, L. Zhang, Y. Wang, Z. Yan, S. Liu, Hierarchically ordered meso/macroporous γ-alumina for enhanced hydrodesulfurization performance, Microporous Mesoporous Mater. 158 (2012) 1–6, https://doi.org/10.1016/j.micromeso.2012.03.022.
[41] G. Prieto, M. Shakeri, K.P. de Jong, P.E. de Jongh, Quantitative relationship between support porosity and the stability of pore-confined metal nanoparticles studied on CuZnO/SiO_2 methanol synthesis catalysts, ACS Nano 8 (3) (2014) 2522–2531, https://doi.org/10.1021/nn406119j.
[42] N. Masoud, T. Partsch, K.P. de Jong, P.E. de Jongh, Thermal stability of oxide-supported Au nanoparticles, Gold Bull. 52 (2019) 105–114.
[43] C.E. Pompe, M. Slagter, P.E. de Jongh, K.P. de Jong, Impact of heterogeneities in silica-supported copper catalysts on their stability for methanol synthesis, J. Catal. 365 (2018) 1–9, https://doi.org/10.1016/j.jcat.2018.06.014.
[44] S. Zhang, M. Cargnello, W. Cai, C.B. Murray, G.W. Graham, X. Pan, Revealing particle growth mechanisms by combining high-surface-area catalysts made with monodisperse particles and electron microscopy conducted at atmospheric pressure, J. Catal. 337 (2016) 240–247, https://doi.org/10.1016/j.jcat.2016.02.020.
[45] E. Ruckenstein, S.H. Lee, The behavior of model Ag/Al_2O_3 catalysts in various chemical environments, J. Catal. 109 (1988) 100–119, https://doi.org/10.1016/0021-9517(88)90188-1.
[46] M. Bowker, Effects of sintering on the active site distribution on promoted catalysts, Appl. Catal. 45 (1) (1988) 115–130, https://doi.org/10.1016/S0166-9834(00)82397-0.
[47] T. Zambelli, J.V. Barth, J. Wintterlin, Formation mechanism of the O-induced added-row reconstruction on Ag(110): a low-temperature STM study, Phys. Rev. B – Condens. Matter Mater. Phys. 58 (19) (1998) 12663–12666, https://doi.org/10.1103/PhysRevB.58.12663.
[48] S.R. Seyedmonir, D.E. Strohmayer, G.J. Guskey, G.L. Geoffroy, M.A. Vannice, Characterization of supported silver catalysts. III. Effects of support, pretreatment, and gaseous environment on the dispersion of Ag, J. Catal. 93 (1985) 288–302, https://doi.org/10.1016/0021-9517(85)90176-9.
[49] A.J.F. van Hoof, R.C.J. van der Poll, H. Friedrich, E.J.M. Hensen, Dynamics of silver particles during ethylene epoxidation, Appl. Catal. B Environ. 272 (2020) 118983, https://doi.org/10.1016/j.apcatb.2020.118983.
[50] J.E. van den Reijen, P.H. Keijzer, P.E. de Jongh, Pore structure stabilization during the preparation of single phase ordered macroporous α-alumina, Materialia. 4 (2018) 423–430, https://doi.org/10.1016/j.mtla.2018.10.016.
[51] M. Matusz, Process for Preparing Ethylene Oxide Catalysts, 1998.
[52] M.S.C. Chan, E. Marek, S.A. Scott, J.S. Dennis, Chemical looping epoxidation, J. Catal. 359 (2018) 1–7, https://doi.org/10.1016/j.jcat.2017.12.030.
[53] M. Nguefack, A.F. Popa, S. Rossignol, C. Kappenstein, Preparation of alumina through a sol-gel process. Synthesis, characterization, thermal evolution and model of intermediate boehmite, PCCP 5 (19) (2003) 4279–4289, https://doi.org/10.1039/B306170A.
[54] W.L. Suchanek, J.M. Garcés, P.F. Fulvio, M. Jaroniec, Hydrothermal synthesis and surface characteristics of novel alpha alumina nanosheets with controlled chemical composition, Chem. Mater. 22 (24) (2010) 6564–6574, https://doi.org/10.1021/cm102158w.
[55] D.L. Perry, Handbook of Inorganic Compounds, 1995. https://doi.org/10.1128/AAC.03728-14.
[56] J. Lu, J. Bravosuarez, A. Takahashi, M. Haruta, S. Oyama, In situ UV-vis studies of the effect of particle size on the epoxidation of ethylene and propylene on supported silver catalysts with molecular oxygen, J. Catal. 232 (1) (2005) 85–95, https://doi.org/10.1016/j.jcat.2005.02.013.
[57] S. Linic, M.A. Barteau, Formation of a stable surface oxametallacycle that produces ethylene oxide, J. Am. Chem. Soc. 124 (2) (2002) 310–317, https://doi.org/10.1021/ja0118136.
[58] M.O. Ozbek, I. Onal, R.A. van Santen, Effect of surface and oxygen coverage on ethylene epoxidation, Top. Catal. 55 (11-13) (2012) 710–717, https://doi.org/10.1007/s11244-012-9870-7.
[59] V. Amendola, O.M. Bakr, F. Stellacci, A study of the surface plasmon resonance of silver nanoparticles by the discrete dipole approximation method: effect of shape, size, structure, and assembly, Plasmonics 5 (1) (2010) 85–97, https://doi.org/10.1007/s11468-009-9120-4.
[60] A. Liebsch, Surface-plasmon dispersion and size dependence of Mie resonance: silver versus simple metals, Phys. Rev. B. 48 (15) (1993) 11317–11328, https://doi.org/10.1103/PhysRevB.48.11317.
[61] Y. Han, R. Lupitskyy, T.M. Chou, C.M. Stafford, H. Du, S. Sukhishvili, Effect of oxidation on surface-enhanced Raman scattering activity of silver nanoparticles: a quantitative correlation, Anal. Chem. 83 (2011) 5873–5880, https://doi.org/10.1021/ac2005839.
[62] G. Boskovic, N. Dropka, D. Wolf, A. Brückner, M. Baerns, Deactivation kinetics of Ag/Al_2O_3 catalyst for ethylene epoxidation, J. Catal. 226 (2004) 334–342, https://doi.org/10.1016/j.jcat.2004.06.003.
[63] B. Delmon, Characterization of catalyst deactivation: industrial and labaratory time scales, Appl. Catal. 15 (1985) 1–16.
[64] A.E.B. Presland, G.L. Price, D.L. Trimm, Particle size effects during the sintering of silver oxidation catalysts, J. Catal. 26 (1972) 313–317.
[65] W.M. Shen, J.A. Dumesic, C.G. Hill, Criteria for stable Ni particle size under methanation reaction conditions: nickel transport and particle size growth via nickel carbonyl, J. Catal. 68 (1981) 152–165, https://doi.org/10.1016/0021-9517(81)90048-8.
[66] N. Masoud, L. Delannoy, H. Schaink, A. van der Eerden, J.W. de Rijk, T.A.G. Silva, D. Banerjee, J.D. Meeldijk, K.P. de Jong, C. Louis, P.E. de Jongh, Superior stability of Au/SiO_2 compared to Au/TiO_2 catalysts for the selective hydrogenation of butadiene, ACS Catal. 7 (9) (2017) 5594–5603, https://doi.org/10.1021/acscatal.7b0142410.1021/acscatal.7b01424.s001.
[67] D. Guo, Q. Guo, K. Zheng, E.G. Wang, X. Bao, Initial growth and oxygen adsorption of silver on Al_2O_3 film, J. Phys. Chem. C 111 (10) (2007) 3981–3985, https://doi.org/10.1021/jp066842n.
[68] C. Petitto, G. Delahay, A new way for silver alumina catalyst preparation, Catal. Lett. 142 (4) (2012) 433–438, https://doi.org/10.1007/s10562-012-0784-6.
[69] D.B. Rasmussen, T.V.W. Janssens, B. Temel, T. Bligaard, B. Hinnemann, S. Helveg, J. Sehested, The energies of formation and mobilities of Cu surface species on Cu and ZnO in methanol and water gas shift atmospheres studied by DFT, J. Catal. 293 (2012) 205–214, https://doi.org/10.1016/j.jcat.2012.07.001.
[70] P. Munnik, M.E.Z. Velthoen, P.E. de Jongh, K.P. de Jong, C.J. Gommes, Nanoparticle growth in supported nickel catalysts during methanation reaction - larger is better, Angew. Chemie. 126 (36) (2014) 9647–9651, https://doi.org/10.1002/ange.201404103.
[71] R. Ouyang, J.-X. Liu, W.-X. Li, Atomistic theory of ostwald ripening and disintegration of supported metal particles under reaction conditions, J. Am. Chem. Soc. 135 (5) (2013) 1760–1771, https://doi.org/10.1021/ja3087054.
[72] G. Prieto, J.D. Meeldijk, K.P. De Jong, P.E. De Jongh, Interplay between pore size and nanoparticle spatial distribution: consequences for the stability of CuZn/SiO_2 methanol synthesis catalysts, J. Catal. 303 (2013) 31–40, https://doi.org/10.1016/j.jcat.2013.02.023.
[73] S.R. Seyedmonir, J.K. Plischke, M.A. Vannice, H.W. Young, Ethylene oxidation over small silver crystallites, J. Catal. 123 (2) (1990) 534–549, https://doi.org/10.1016/0021-9517(90)90149-E.
[74] W.E. Evans, P.I. Chipman, Process for operating the epoxidation of ethylene, WO2001096324A2, 2001.
[75] S.T. Oyama, Mechanisms in Homogeneous and Heterogeneous Epoxidation Catalysis, first ed., Elsevier B.V, 2008.
[76] R.E. Kenson, M. Lapkin, Kinetics and mechanism of ethylene oxidation. Reactions of ethylene and ethylene oxide on a silver catalyst, J. Phys. Chem. 74 (7) (1970) 1493–1502.
[77] J.E. van den Reijen, W.C. Versluis, S. Kanungo, M.F. d'Angelo, K.P. de Jong, P.E. de Jongh, From qualitative to quantitative understanding of support effects on the selectivity in silver catalyzed ethylene epoxidation, Catal. Today 338 (2019) 31–39, https://doi.org/10.1016/j.cattod.2019.04.049.

[78] J.H. Miller, A. Joshi, X. Li, A. Bhan, Catalytic degradation of ethylene oxide over Ag/α-Al_2O_3, J. Catal. 389 (2020) 714–720, https://doi.org/10.1016/j.jcat.2020.07.008.
[79] J. JANKOWIAK, M. BARTEAU, Ethylene epoxidation over silver and copper-silver bimetallic catalysts: II. Cs and Cl promotion, J. Catal. 236 (2) (2005) 379–386, https://doi.org/10.1016/j.jcat.2005.10.017.
[80] J.C. Dellamorte, J. Lauterbach, M.A. Barteau, Rhenium promotion of Ag and Cu-Ag bimetallic catalysts for ethylene epoxidation, Catal. Today 120 (2) (2007) 182–185, https://doi.org/10.1016/j.cattod.2006.07.051.
[81] J. Jankowiak, M. Barteau, Ethylene epoxidation over silver and copper-silver bimetallic catalysts: I. Kinetics and selectivity, J. Catal. 236 (2) (2005) 366–378, https://doi.org/10.1016/j.jcat.2005.10.018.
[82] A.R. Fiorucci, L.M. Saran, É.T.G. Cavalheiro, E.A. Neves, Thermal stability and bonding in the silver complexes of ethylenediaminetetraacetic acid, Thermochim Acta 356 (1-2) (2000) 71–78, https://doi.org/10.1016/S0040-6031(00)00478-0.
[83] P. Petit, D. Salem, M. He, M. Paillet, R. Parret, J.-L. Sauvajol, A. Zahab, Study of the thermal stability of supported catalytic nanoparticles for the growth of single-walled carbon nanotubes with narrow diameter distribution by chemical vapor deposition of methane, J. Phys. Chem. C 116 (45) (2012) 24123–24129, https://doi.org/10.1021/jp307618h.
[84] D.L. Trimm, Thermal stability of catalyst supports, Stud. Surf. Sci. Catal. 68 (1991) 29–51, https://doi.org/10.1016/S0167-2991(08)62619-1.